Surface & Coatings Technology 395 (2020) 125929

Contents lists available at ScienceDirect

Surface & Coatings Technology

journal homepage: www.elsevier.com/locate/surfcoat

Magnesium scaffolds with two novel biomimetic designs and MgF_2 coating for bone tissue engineering

Saeid Toghyani[a,*], Mohammad Khodaei[b], Mehdi Razavi[c]

[a] Young Researchers and Elite Club, Isfahan (Khorasgan) Branch, Islamic Azad University, Isfahan, Iran
[b] Department of Materials Science and Engineering, Golpayegan University of Technology, Golpayegan, Iran
[c] BiionixTM (Bionic Materials, Implants & Interfaces) Cluster, Department of Internal Medicine, College of Medicine, University of Central Florida, Orlando, FL 32827, USA

ARTICLE INFO

Keywords:
Magnesium scaffold
Sucrose spacer agent
Mechanical properties
MgF_2 coating
Biodegradability

ABSTRACT

In this study, magnesium scaffolds including 60% porosity were designed and fabricated using sucrose spacer agent by the powder metallurgy technique with the pore size of 400–600 μm with two biomimetic designs of the filled center design (FCD) and the hollow center design (HCD) for bone regeneration. The spacer agent was removed by distilled water and hydrofluoric (HF) acid before the sintering process. After the sintering process, on the surfaces of both scaffold designs, magnesium fluoride (MgF_2) coating was applied. Evaluation of scaffolds by X-ray diffractometery (XRD) show that, on the surface of the untreated scaffolds MgF_2 had been negligible formed because of spacer agent removal process using HF solution. However, on the surface coated magnesium scaffold a thicker coating of $MgF_2$was formed. Results of compression test showed that by changing the design from hollow center to filled, the yield stress of the scaffolds increased from 7.3 MPa to 22 MPa. In addition, *in vitro* test indicated that both designs of MgF_2 coated magnesium scaffolds had approximately same degradation rates. Also, the results of magnesium ion release by ICP-AES test showed that the MgF_2 coated magnesium scaffolds had lower degradation rate compared to uncoated scaffolds. In addition, EDS analysis on the surface of the coated magnesium scaffold confirms the formation of MgF_2 coating. Also, this analysis showed that after 14 days of immersion in Dullbecco's PBS solution, the MgF_2 layer remained on the surface of the scaffold.

1. Introduction

Porous biomaterials called 3D scaffolds are currently under investigation for bone regeneration. The ideal biomaterial to develop these bioscaffold needs to have following characteristics: Biocompatible and biodegradable, [1–3], a matched elastic modulus to natural bone to reduce or remove the stress shielding effect [4–7], and a controlled degradation rate or corrosion resistance [8,9]. Many studies have demonstrated that magnesium has the aforementioned properties making it a promising biomaterial for bone regeneration, except its high corrosion rate [10–12], which is considered as its main limitation. Previous research on magnesium scaffolds have shown that if the scaffold porosity is reduced to 20%, its corrosion rate can be partially reduced [13,14]. However, magnesium scaffolds with 20% porosity had no significant interconnected pores [13]. To provide sufficient interconnected pores for adequate oxygen and nutrient transport, metabolic waste excretion, and blood vessel growth [15], magnesium scaffold requires to have a higher percentage of porosity (*i.e.* 50–80%). As a result, many *in vitro* and *in vivo* experiments have shown that surface coating or modification can be used as an effective and practical method to overcome the corrosion limitations of magnesium scaffolds. Different coatings have also been used such as MgF_2 [8,16], polycaprolactone [17], polycaprolactone/bioactive glass composite [18], multilayer coatings of polycaprolactone-bioactive glass/gelatin-bioactive glass (PCL–BaG/Gel–BaG) [19], hydroxyapatite (HA) [12], HA coating layer and hybrid (PEI)–SiO_2 layers [20], micro-arc oxidation (MAO) [11], MAO and gelatin coating [3], and β−tricalcium phosphate (β–TCP) coating [2]. In general, coating methods are effective on the physicochemical properties of the surface and consequently the bone-to-implant interactions. A coating like MgF_2 besides improving the corrosion resistance of magnesium, results in an improved biocompatibility and also antibacterial activity of magnesium substrate [21–23]. In addition, beneficial effects of fluoride incorporation, have been reported before; these effects include stimulating osteoblast proliferation, promoting bone formation, and preventing osteoporosis-related fractures [16,24]. As one of the scaffold manufacturing methods,

* Corresponding author.
E-mail address: s.toghyani@khuisf.ac.ir (S. Toghyani).

https://doi.org/10.1016/j.surfcoat.2020.125929
Received 9 March 2020; Received in revised form 12 May 2020; Accepted 15 May 2020
Available online 16 May 2020
0257-8972/

Table 1
Advantages and disadvantages of carbamide, ammonium bicarbonate and sodium chloride as spacer agents for the fabrication of metal scaffolds.

Spacer agent	Advantages	Disadvantages	References
Carbamide	Soluble in water (1000 g/L), ethanol and hydrofluoric acid	It is not completely removed by water and ethanol for an optimal immersion time Its residue is not removed up to the T_m of magnesium	[9,10,32]
Ammonium bicarbonate	Soluble in water (220 g/L)	Its residue is not removed up to the T_m of magnesium from the center of the scaffold When heated, it releases ammonia and water	[31,33]
Sodium chloride	Soluble in water (360 g/L) and biocompatible	NaCl solutions at different concentrations can results in metal corrosion Causes foam cracking and delamination during sintering stage	[6,28,29,34]

the powder metallurgy has been extensively used since it is simple and cost-effective. In this method most particles of carbamide [25–27], sodium chloride [28,29], or ammonium bicarbonate [30,31] have been used as spacer agent. However, an important step in fabrication process is to completely remove the spacer agent prior to the sintering process [10]. Because, according to Table 1, the spacer agents particles cannot be completely removed during the sintering process (mainly from the center of the scaffold) and also decomposition product release that can lead to the oxidation or contamination of magnesium.

Therefore, in addition to a need for the use of a high soluble spacer agent, unique designs are required to remove spacer agent from the scaffold center prior to the sintering process. As a result, in this study with the idea of two biomimetic designs, pure magnesium scaffolds were first fabricated using sucrose particles as a spacer agent and then coated with magnesium fluoride. Our results showed that the fabricated magnesium scaffolds were free of contaminations caused by spacer agent particles, as well as the coating of scaffolds with MgF_2 coating reduced the corrosion rate of our magnesium scaffolds.

2. Materials and methods

2.1. Materials

Magnesium scaffolds were fabricated using powder metallurgy method. Magnesium powder (Merck: CAS 7439-95-4) with particles size of smaller than 70 μm and crystal powder of sucrose ($C_{12}H_{22}O_{11}$: Merck: 1076531) with particles size at the range of 400–600 μm were used as the spacer agent, (Fig. 1).

2.2. Magnesium scaffold fabrication

Magnesium scaffolds were fabricated in two different designs of hollow center and filled center. At the filled center design (FCD), the center of sample consisted of a prefabricated magnesium rod with a purity of 99.9% (D = 2 mm, H = 25 mm), which was surrounded by a porous magnesium scaffold (D = 8 mm, H = 8 mm, porosity of 60 vol %). At the hollow center design (HCD), the hollow center of sample was 2 mm in diameter. Fig. 2 presents the schematic of scaffolds fabrication routes. To fabricate the HCD magnesium scaffold, a rod shape hardened steel (D = 2 mm, H = 25 mm) was fixed at the center of cylindrical steel mold (D = 8 mm, H = 24 mm) by a steel pellet of hollow center (D = 7.98 mm, H = 3 mm), and the space between them was filled by mixture of 40 vol% magnesium powder and 60 vol% sucrose. The mixture was compressed using a hollow center punch that the rod passes easily through it, up to 400 MPa pressure for 2 min. Then, a rod shape hardened steel (D = 1.90 mm) was placed from the top within the steel punch hole where the powders mixture had been pressed. The rod shape hardened steel that had been fixed in the sample center was pushed out by the force of the cold press machine. The compacted pellet was then removed from the mold.

To fabricate the FCD magnesium scaffold, a prefabricated magnesium rod was placed in the center of cylindrical steel mold and the gap between them was filled by mixture of 40 vol% magnesium powder and 60 vol% sucrose. The mixture was compressed same as the procedure described above for the HCD sample. The compacted pellet was then removed from the mold, and the excess height of the surrounded magnesium rod within the center of the sample was then cut by the saw. To remove the spacer agent from both FCD and HCD pellets, they were immersed in double distilled water for to 2 h at room temperature. To ensure complete removal of spacer agent and prevent magnesium corrosion in water for longer immersion time, we immersed them in HF 48% for 5–10 min. Samples were finally kept at 40 °C for 24 h to be dried), and then sintered at 630 °C for 2 h, at inert atmosphere under high purity argon gas. The heating rate in sintering process was 5 $°C \cdot min^{-1}$.

2.3. Magnesium scaffold coating

Magnesium fluoride was coated on the surface of FCD and HCD magnesium scaffolds to reduce their corrosion rate. For this purpose, the uncoated scaffolds were immersed in HF 48% at ambient temperature for 15 h, then removed, rinsed with ethanol and dried at 40 °C for 24 h.

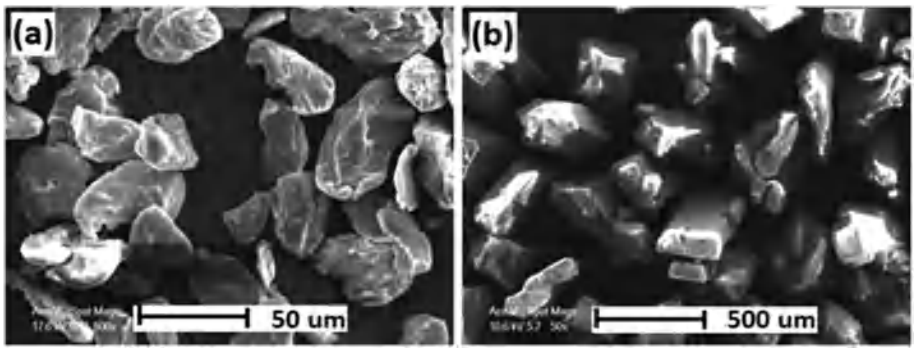

Fig. 1. SEM micrograph of initial materials: (a) magnesium powder, (b) spacer agent particles of sucrose.

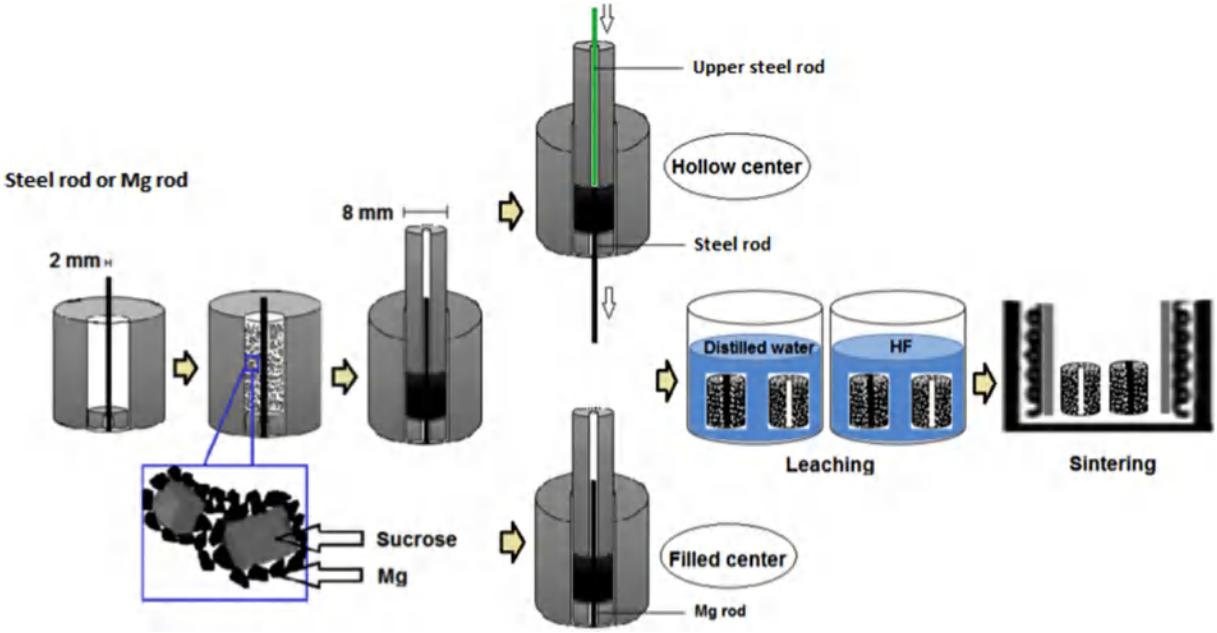

Fig. 2. Schematic of FCD and HCD magnesium scaffold fabrication processes.

2.4. Magnesium scaffold characterization

2.4.1. SEM and EDS analysis

Scanning electron microscopy (SEM: Philips XL-30) equipped with an energy dispersive spectroscopy (EDS) was used to observe the microstructure and pore morphology of coated and uncoated magnesium scaffolds, determine the thickness of the deposited MgF_2 coating on the scaffold surfaces and identify the chemical elements within the coating. Samples were gold coated using sputter coater to inhibit electron charge.

2.4.2. XRD analysis

To determine the phases of both uncoated and coated magnesium scaffolds, X-ray diffraction (XRD: Philips, X'Pert-MPD, Netherland) was used as the radiation source of Cu-K_α (λ = 1.5405 A°), at 40 KV, at the rate of 1°/min in the range of 2θ = 25–70°.

2.4.3. Porosity evaluation

The porosity of magnesium scaffolds were calculated by Eqs. (1) and (2), respectively.

$$P_{F.HC} = \left(1 - \frac{M_F/V_F}{\rho_{Mg}}\right) \times 100 \quad (1)$$

$$P_{F.FC} = \left(1 - \frac{M_F - M_c/V_F}{\rho_{Mg}}\right) \times 100 \quad (2)$$

where, $P_{F.\ HC}$ and $P_{F.\ FC}$ are the actual porosity hollow center and filled center scaffolds, respectively. M_F and M_c the weight of the porous area of the scaffold and the weight of the located magnesium rod in the center of the scaffold, respectively. V_F is the volume of porous area of the designed scaffolds. The weight and dimensions of the samples were measured using a digital balance with 0.0001 g precision and a digital caliper with a precision of 0.01 mm, respectively. ρ_{Mg} is the density of pure bulk magnesium (1.74 g/cm^3).

2.4.4. Mechanical properties assessment

To evaluate the mechanical properties of FCD and HCD magnesium scaffolds, compression test for cylindrical samples of (D = 8 mm, H = 8 mm) was performed using Universal Testing Machine (INSTRON 5566S, USA), according to ISO 13314: 2011 at a cross-speed of 1 mm/min. The compression test was repeated three times for each sample and average values are reported.

2.4.5. In vitro degradation behavior

To study and compare the degradation behavior, FCD and HCD magnesium scaffolds (both coated and uncoated groups; D = 4 mm, H = 4 mm), were immersed in the Dulbecco's Phosphate Buffered Saline (DPBS; 25 ml) at 37 °C for 21 days; finally the magnesium ion concentration and the pH value of DPBS were measured using inductively coupled plasma mass spectrometry (ICP-MS: HITACHI, PS7800, Japan) and pH meter (pH & ION meter Systronics 808), respectively. Also, weight loss of the dried specimens was evaluated by weight difference before and after immersion at two time points of 1 and 14 days. After removal of corrosion products from the surface of specimens by chromium trioxide solution (CrO_3) according to ASTM G1-90 [35], the samples were washed with alcohol and finally dried at 40 °C for 24 h.

2.5. Statistical analysis

Quantitative data of compression tests, porosity measurement and degradation behavior are repeated for 3 times and the results presented as mean ± standard deviation. Statistical analysis was carried out using IBM SPSS Statistics 23 software, and *P* value of smaller than 0.05 was considered significant.

3. Results and discussion

3.1. Sucrose removal

Results of sucrose removal inside the magnesium scaffolds with 60% porosity in both designs of hollow center and filled center by measuring the weight of the dry samples before and after the dissolution process showed that after 2 h immersing in double distilled water, 93 ± 2% and 88 ± 2% of spacer agent particles have been removed, respectively. Hence, it is clearly evident that in hollow center design, more spacer agent particles are removed when compared to the filled center design, which is due to the more access of the hollow center to double distilled water and diffusion of double distilled water into the pores

structure. On the other hand, water is released following the thermal decomposition of sucrose [36], that can react with magnesium at high temperatures. Furthermore, it is essential for the spacer agent particles of sucrose to be removed as much as possible before the sintering process. Therefore, after dissolution by double distilled water, to ensure complete removal of spacer agent, samples were immersed in 48% HF solution for 5–10 min. Results of samples immersion in 48% HF solution showed that the spacer agent particles residue inside the pores were removed same up to 98 ± 2% for both samples. Generally, the solubility of sucrose in water at the temperature of 20 °C reaches to 2100 g/L [37], which is significantly higher than the solubility of other spacer agents used in the fabrication of magnesium scaffolds. While, the solubility of spacer agents used in the fabrication of magnesium scaffolds, such as ammonium bicarbonate (NH_4HCO_3), sodium chloride (NaCl) and carbamide (CH_4N_2O) in water at ambient temperature or at 20 °C is approximately 220, 360 [34,68] and 1000 g/L [32,63], respectively. As a result, it can be concluded that the removal of sucrose spacer agent particles by dissolution process can be more efficient than other commonly spacer agent particles used in the fabrication of porous magnesium scaffolds.

3.2. Microstructure and morphology of magnesium scaffolds

The uncoated sintered Mg scaffolds with FCD and HCD designs are shown in Fig. 3. According to Fig. 3(a-b) the fabricated scaffolds have metallic shine and are free of impurities detectable by the naked eyes. Fig. 3(c-d) shows the SEM micrographs of the surfaces of the magnesium scaffolds with hollow center design or filled center. In Fig. 3(c) it is clearly evident that the center of the scaffold is hollow with 2 mm in diameter. Also, in Fig. 3(d) it is clearly evident that a good bond is formed between the dense central and porous areas and no discontinuity and crack is observed between them. In addition, almost uniform distribution in spacer particles is seen in Fig. 3(c-d). This leads to a highly interconnected pores which facilitate bone cells to migrate into the scaffold and reconstruct the damaged tissue [9]. Our hollow center design along with the uniform distribution of pores can be an effective strategy to improve the coating efficiency of porous scaffolds. Because, the empty space of the sample center can be a way for the coating material to enter the pores of the scaffold. Using this hollow-types techniques, uniform multilayer coatings can also be applied on the surface of magnesium scaffolds to overcome their corrosion problem. More importantly, if the residue of the spacer particles are not fully removed from the scaffold, they can stick to the walls; and in addition to reducing the implant biocompatibility, it prevents the formation of uniform and continuous coatings on the scaffold surfaces. Fig. 4 Shows the SEM image and EDS elemental analysis from the cross-section of the scaffold coated with magnesium fluoride. According to Fig. 4, a very thin layer of magnesium fluoride with a thickness of about

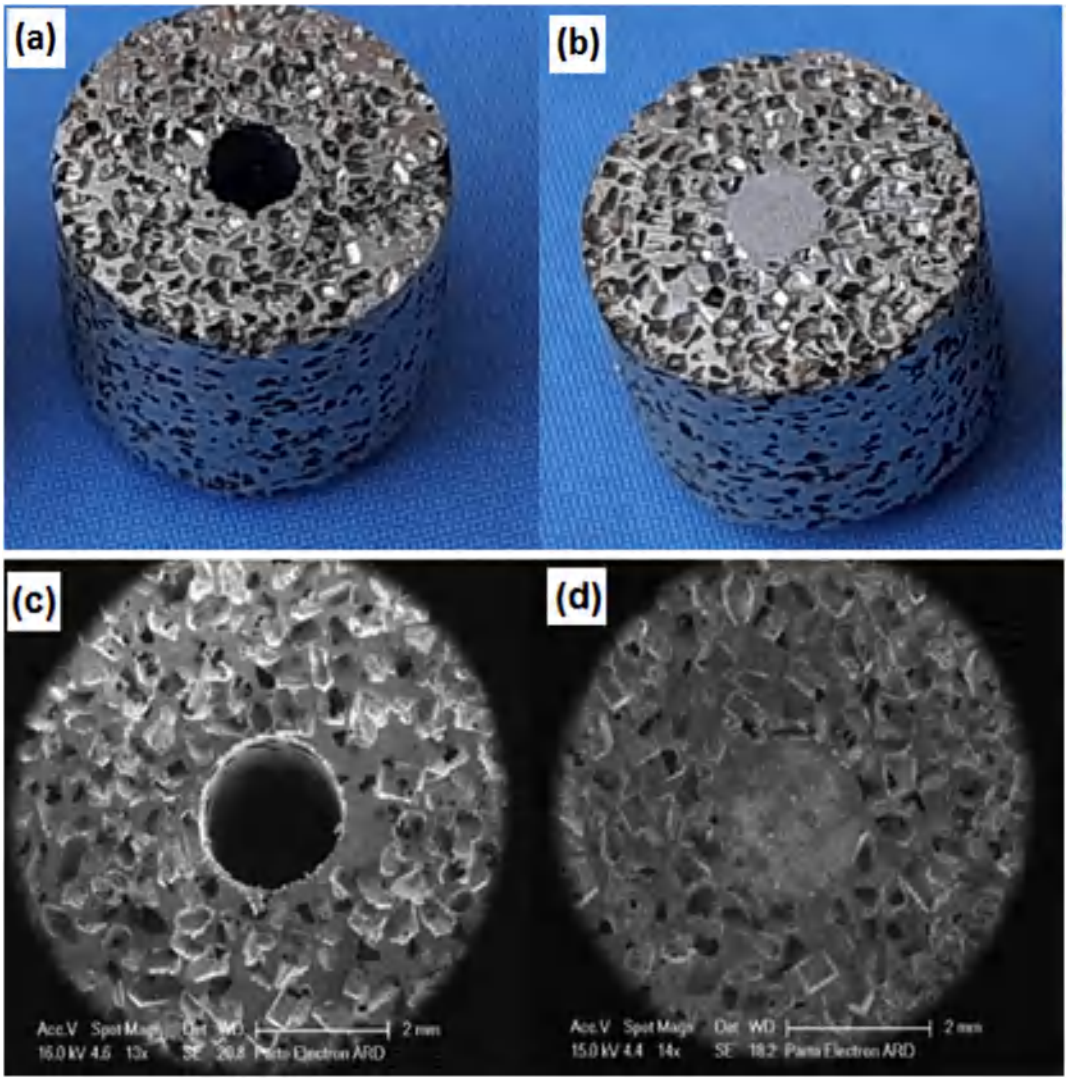

Fig. 3. Photos (a-b) and SEM micrographs (c-d) of magnesium scaffolds with HCD (a, c) and FCD (b, d) designs.

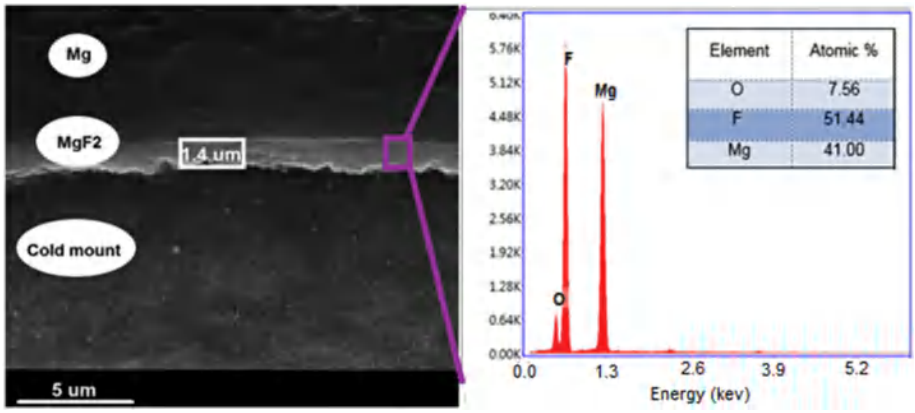

Fig. 4. SEM micrograph and EDS of the surface of MgF_2 coated magnesium scaffold.

1.4 μm is seen on the surface of the magnesium scaffold. This magnesium fluoride coating had been formed on the surface of magnesium scaffolds following their immersion in HF solution for 15 h. Also, the results of the EDS analysis show that the atomic ratio of fluoride to magnesium is almost matches to the atomic ratio of magnesium to fluoride. In general, this coating is formed by the reaction of magnesium with HF as shown in Eq. (3). This reaction has a negative change in the Gibbs free energy, indicating that this is a product formed at the temperature of 298.15 K [21].

$$Mg(s) + 2HF(aq) \rightarrow MgF_2(s) + H_2(g)\ \Delta G = -476.6\ kJ/mol \quad (3)$$

Zhang et al. [38], showed that by the immersing the Mg-Nd-Zn-Zr magnesium alloy in 40% HF solution for 24 h, a layer of magnesium fluoride with thickness of 1.5 μm is formed on the magnesium substrate. Also, Makkar [39], showed that by the immersing the ZK60 magnesium alloy in 48% HF solution for 24 h at room temperature, a layer of magnesium fluoride with a thickness of approximately 2.2 μm was formed on the magnesium substrate. Chiu et al. [22] also coated a 1.5 μm thick magnesium fluoride on pure magnesium by immersing them in 48% HF solution for 24 h at room temperature. In addition, researchers have interpreted that as the thickness of the MgF_2 layer increases, the rate of coating process decreases whereafter 70 h of immersion, the magnesium fluoride coating reaches its maximum thickness of 2.75 μm [40].

3.3. Characterization of magnesium scaffolds surfaces

The X-ray diffraction (XRD) patterns for uncoated and MgF_2 coated magnesium scaffolds are presented in Fig. 5. Both patterns are mainly containing magnesium peaks with hexagonal structure. With the difference that in uncoated scaffolds, very small peaks (negligible) of magnesium fluoride (Sellaite) with tetragonal structure has been formed on the scaffold surfaces during spacer leaching in HF for 5–10 min. In addition, in MgF_2 coated scaffolds, with greater intensity magnesium fluoride peaks appeared. In general, the low intensity of magnesium fluoride peaks indicates that this coating is very thin. On the other hand, it is demonstrated that, during the magnesium sintering under a protective atmosphere (vacuum or argon), MgF_2 cannot be decomposed, because of the high temperatures *i.e.* > 800 °C which is required for oxidation of MgF_2 and conversion to MgO in air [41]. Also, in our XRD patterns, a small peak at 43° was detected in both samples, which is related to magnesium oxide. This magnesium oxidation might be formed due to the sample immersion in water for 2 h.

3.4. Porosity of magnesium scaffolds

Due to shrinkage of the scaffolds during the sintering process at temperature of 630°C, dimensions of scaffolds with hollow center and filled center decreased by 6% and 4%, respectively. More dimension change of the hollow center magnesium scaffolds can be due to the 2 mm gap in the center of the specimens. Nevertheless, the actual porosity of magnesium scaffolds with HCD and FCD designs compared to the theoretical porosity of the scaffolds decreased by 4% and 2% respectively. This difference between theoretical porosity and actual porosity of scaffolds can be due to the closure of micropores during the sintering process.

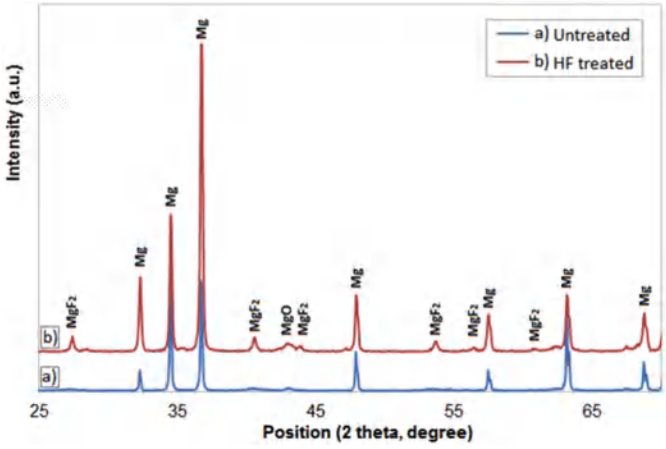

Fig. 5. X-ray diffraction patterns for: (a) uncoated magnesium scaffold, (b) MgF_2 coated magnesium scaffold.

3.5. Mechanical properties of magnesium scaffolds

Results of the mechanical properties for both magnesium scaffold designs are presented in Fig. 6. Results shows that, the compressive strength and yield stress of filled center scaffolds are approximately three times higher than center scaffolds The (yield stress: 22 MPa *vs* 7.3 MPa, the plateau stress 19.5 MPa *vs* 7.7 MPa to). Since the compressive strength of pure magnesium is approximately 200 MPa [42], inserting a rod with a diameter of 2 mm in the center will increase to the strength around 12.5 MPa, this is matched the obtained difference between the strength of the filled and hollow center scaffolds.

In Table 2, the mechanical properties of the trabecular bones (spongy) are compared with the mechanical properties of our fabricated scaffolds and also other magnesium scaffolds made with ≥50% porosity based on the literature. It is clearly evident that a scaffold with a combination of interconnected porous and dense areas has a higher strength than a scaffolds with 50% porosity or a scaffold with hollow center. However, normal scaffolds or hollow-center scaffolds in addition to preserving the biological benefits of the porous structure they

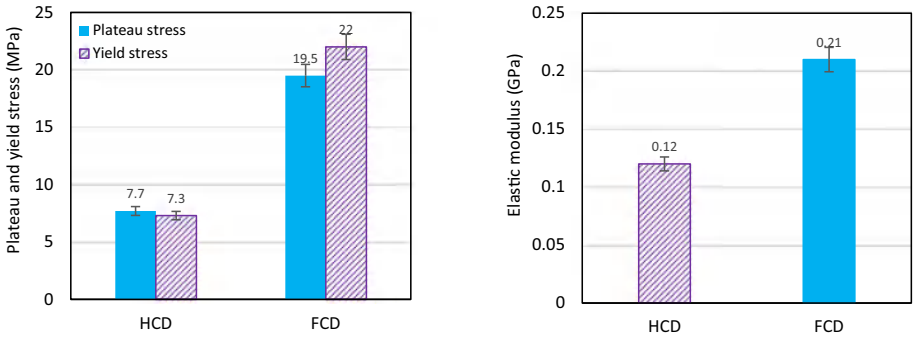

Fig. 6. Mechanical properties of fabricated magnesium scaffolds with FCD and HCD designs.

can be sufficiently strong. Because, it is proven that the bones of load bearing in human body have different mechanical properties. So that, the loads for breaking the patella, tibiae, humerus, and femur bones are about 192, 450, 600, and 756 kg, respectively [43]. Generally speaking, there are different types of bone in human body, which most of them consisted of cortical and cancellous zones. Every types of bone have different thickness in cortical section, resulting different loadbearing ability [44]. As a result, fabricated scaffolds with both designs in the present study can be used in places with the compressive forces required for growth and regeneration of broken load-bearing bone.

3.6. In vitro degradation properties of magnesium scaffolds

Changes in magnesium ion concentration of Dullbecco's PBS solution by immersion of both groups of uncoated and MgF_2 coated scaffolds with FCD and HCD designs at time points of 12 h, 1, 3, 8, 14, and 21 days, are plotted in Fig. 7. Uncoated magnesium scaffolds with both designs released more magnesium ions compared to MgF_2 coated scaffolds. This means that, uncoated scaffolds have a faster degradation. Following the immersion of the uncoated magnesium scaffolds, the amount of magnesium ion release significantly increased and then reached a steady state after 8 days. Similarly, the amount of released magnesium ion from the coated scaffolds gradually increased over the time. However, coated scaffolds with both FCD and HCD designs, had approximately the same magnesium ion release after 21 days of immersion in Dullbecco's PBS solution at 37 °C. For the coated scaffolds with HCD design, although they had a higher contact surface area with Dullbecco's PBS solution, they maintained their structural stability for up to 21 days, similar to coated scaffolds with HCD design. However, uncoated magnesium scaffolds with both FCD and HCD designs lost their structural stability after 8 days of immersion. Also, the amount of released magnesium ions from the coated scaffolds into the solution even after 8 days was lower than the amount of magnesium ion released from the uncoated scaffolds after 12 h immersion. This is because of the magnesium fluoride coating which protected the magnesium scaffold

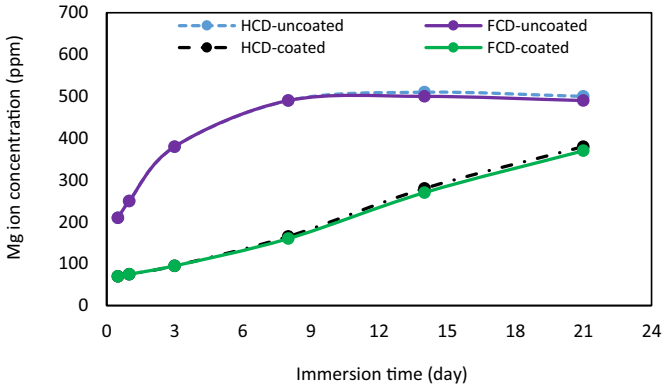

Fig. 7. Concentrations of released Mg ion from uncoated and MgF_2 coated scaffolds with FCD and HCD designs in Dullbecco's PBS solution at different time points.

substrate from exposure to the solution even after 8 days immersion. The magnesium fluoride (MgF_2) is insoluble in water however, it can be dissolved in solutions including chloride ions [47]. Zhang et al. reported that, Mg-Nd-Zn-Zr alloy immersion in DMEM solution up to 10 days resulted in magnesium fluoride coating decomposition after 10 days [38]. Also, previous research indicate that the magnesium fluoride coating besides improving the corrosion resistance of magnesium, improved the biocompatibility of the magnesium since it is nontoxic and also antibacterial [21–23]. It has also been reported that AZ31 magnesium alloy scaffolds coated with magnesium fluoride resulted in an improved proliferation and attachment of rat bone marrow stromal cells (rBMSCs) [16]. Also, extracts taken from magnesium fluoride coated AZ91 scaffold have increased the bone differentiation of rat bone marrow stromal cells. In contrast the uncoated scaffolds had poor cell proliferation and attachment due to excessive release of magnesium ions as a result of rapid degradation [16].

Table 2
Summary of the mechanical properties of the porous Mg scaffolds with porosity of ≥50%, and fabricated magnesium scaffolds in the present study compared to the trabecular bones.

Material type	Porosity (%)	Compressive strength (MPa)	Elastic modulus (GPa)	Ref.
Cancellous bone	–	4–12	0.1–0.5	[2]
Human trabecular bone	50–90	0.2–80	0.01–2	[20]
Fabricated Mg scaffolds with porosity ≥ 50%				
Mg scaffold fabricated by carbamide spacer agent	50	2.33	0.35	[26]
Mg scaffold fabricated by carbamide spacer agent	55	12	0.8	[45]
Mg scaffold fabricated by the fiber deposition hot pressing technology	54	11.1	0.1	[46]
Mg scaffold fabricated by laser perforation	51	8	0.41	[2]
Mg scaffold fabricated by carbamide spacer agent	52–70	4–14	–	[27]
Mg scaffold fabricated by SPS and NaCl spacer agent	60–70	7–15	0.23–0.33	[12]
Our FCD magnesium scaffold	60	19.5	0.21	
Our HCD magnesium scaffold	60	7.7	0.12	

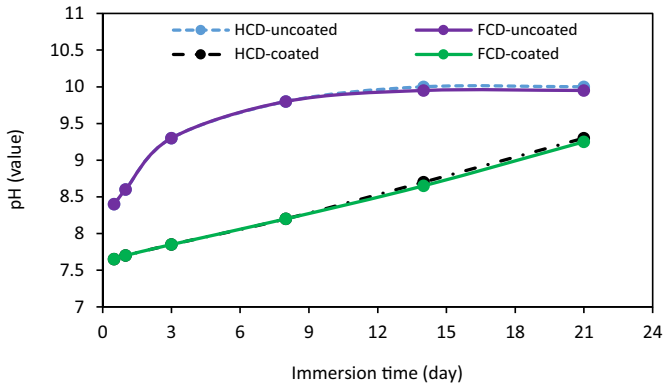

Fig. 8. pH changes of Dullbecco's PBS solution, by immersion of uncoated and MgF_2 coated scaffolds with FCD and HCD designs at different time points.

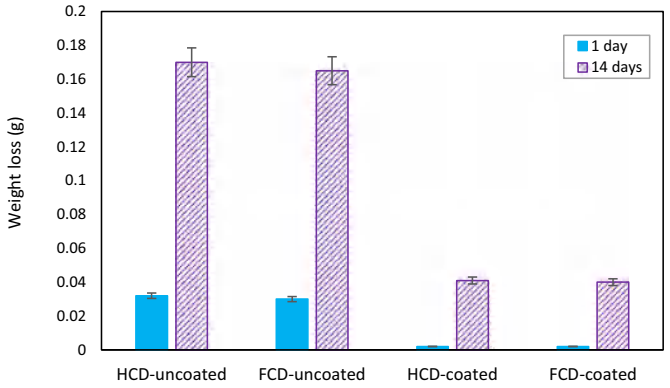

Fig. 9. Weight loss for both groups of uncoated and including MgF_2 coating scaffolds with FCD and HCD designs, at two time points of 1 day and 14 days.

Fig. 8 presents the pH changes of Dullbecco's PBS solution, following immersion of uncoated and MgF_2 coated scaffolds with FCD and HCD designs at different time points. It is evident that the pH value forms the uncoated scaffolds, increased from 7.4 to 8.6 after 1 day of immersion, and gradually increased to 9.3 after 3 days of immersion. Also, with increasing the immersion time from 3 days to 8 days, the pH increased and then reached a steady state. While the pH value of the coated scaffolds gradually increased to 9.3 after 21 days. The pH increase of solution, is related to the magnesium degradation and subsequent release of OH^- functional groups. Following reactions summarizes the degradation process of magnesium in physiological mediums such as Dullbecco's PBS [25,48]:

$$Mg \rightarrow Mg^{2+} + 2e^- \quad (4)$$

$$2H_2O + 2e^- \rightarrow 2OH^- + H_2\,(g) \quad (5)$$

$$Mg^{2+} + 2OH^- \rightarrow Mg(OH)_2 \quad (6)$$

$$Mg(OH)_2\,(s) + 2Cl^-\,(aq) \rightarrow MgCl_2 + 2OH^- \quad (7)$$

The reaction between magnesium and PBS, results in $Mg(OH)_2$ and H_2 gas formation (Eqs. (4), (5) and (6)). $Mg(OH)_2$ is partially insoluble in water and its formation on the surface of magnesium, protect magnesium from corrosion in water [49]. However, it accelerates the corrosion of Mg when the pH is lower than 11.5 [50]. Also, magnesium hydroxide layer, is degraded in PBS, because of chlorine ion of PBS and pH in body fluid which is about 7.5 or even lower, $Mg(OH)_2$ transform to $Mg(Cl)_2$, which is highly soluble in water (Eq. (7)). The burst increase in pH because of OH functional group release has also been reported by other researchers [13,48]. Magnesium scaffolds with both FCD and HCD designs had similar degradation rates pH increase. Also, coated magnesium scaffold reduced the degradation rate and pH increase when compared to uncoated ones. Nevertheless, it has been reported that pH values in the range of 7.9–8.27 do not prevent proliferation of hBMSCs [51].

The weight loss of both groups of uncoated and MgF_2 coated scaffolds with FCD and HCD designs at two time points of 1 and 14 days are shown in Fig. 9. The results shows that the weight of the coated scaffolds reduced after 1 day of immersion, however the weight loss was insignificant. Whereas, uncoated magnesium scaffolds showed a significant weight loss which can be due to the direct exposure of scaffold the physiological medium. The results showed that the uncoated scaffolds with both FCD and HCD designs had greater weight loss compared to the coated scaffolds. So that, the coated scaffolds lost approximately 0.04 g after 14 days of immersion.

SEM images and elemental analysis (EDS) of the surfaces morphology of coated and uncoated magnesium scaffolds, after 14 days of immersion, are shown in Fig. 10. According to Fig. 10(a), the surface of the coated magnesium scaffold has not been extremely degraded so that the pores have maintained their shape in the form of polyhedral structures (*i.e.* the shape of our spacer particles). Although microcracks are observed within the Mg particles, the scaffold structure and mechanical stability has been completely maintained. EDS analysis showed that the corrosion products contains calcium, oxygen, fluoride, magnesium and phosphorus. Fig. 10(b) shows the surface of the uncoated magnesium scaffold which had been highly corroded and the scaffold structure was collapsed. Also, corrosion products contains chlorine, oxygen, and magnesium. Calcium is detectable in our EDS analysis which can be due to the deposition of calcium phosphate products from ions in physiological solution. Also, the phosphate and calcium in solution react with the OH^- ions and forms calcium phosphates such as hydroxyapatite [$Ca_{10}(PO_4)_6(OH)_2$] [23] or fluoridated hydroxyapatite [FHA, $Ca_5(PO_4)_3(OH)_{1-x}F_x$)] [52] on the surface. On the other hand, existence of fluoride in our magnesium fluoride coating can improve calcium phosphate crystallization and mineralization which can also encourage formation of new bone tissue [23,53]. In general, MgF_2 coated scaffolds had less degradation rate than uncoated scaffolds. Because the presence of this coating, it significantly postponed the degradation of the magnesium substrate.

4. Conclusion

In this study, biodegradable magnesium scaffolds were first fabricated using the sucrose spacer agent with two biomimetic designs (the filled center design (FCD) and the hollow center design (HCD)) and then coated using MgF_2. The results show that, sucrose is an appropriate spacer agent for the fabrication of magnesium scaffolds and has no side effects. Also, the results of compression test showed that by changing the design from hollow center to filled, the yield stress and compressive strength of the filled center scaffolds increased approximately three times. The results show that MgF_2 coating significantly reduces the degradation rate of magnesium scaffolds for both HCD and FCD designs. Based on the *in vitro* results of this study, these new microstructural designs of magnesium scaffold with MgF_2 coating by having mechanical properties comparable to bone tissue can overcome the corrosion limitation of magnesium and make it a suitable magnesium-based scaffold for bone tissue regeneration.

Declaration of competing interest

The authors certify that they have NO affiliations with or involvement in any organization or entity with any financial interest or non-financial interest in the subject matter or materials discussed in this manuscript.

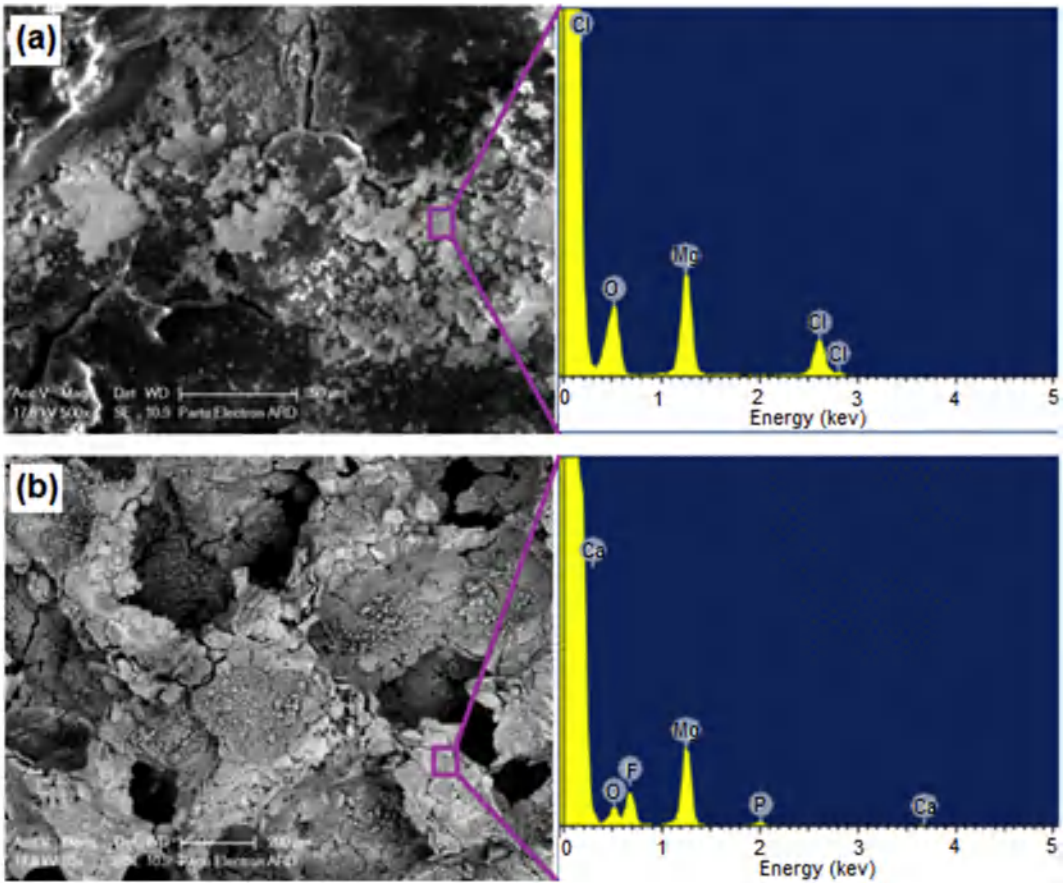

Fig. 10. SEM images and EDS from surfaces of: (a) uncoated magnesium scaffold, (b) MgF_2 coated magnesium scaffold, after 14 days immersion in Dullbecco's PBS solution.

References

[1] P. Han, P. Cheng, S. Zhang, C. Zhao, J. Ni, Y. Zhang, W. Zhong, P. Hou, X. Zhang, Y. Zheng, Yimin Chai, In vitro and in vivo studies on the degradation of high-purity Mg (99.99wt.%) screw with femoral intracondylar fractured rabbit model, Biomaterials 64 (2015) 57–69.

[2] F. Geng, L. Tan, B. Zhang, C. Wu, Y. He, J. Yang, K. Yang, Study on β-TCP coated porous Mg as a bone tissue engineering scaffold material, Mater. Sci. Technol. 25 (1) (2009) 123–129.

[3] Q. Li, G. Jiang, D. Wang, H. Wang, L. Ding, G. He, Porous magnesium loaded with gentamicin sulphate and in vitro release behavior, Mater. Sci. Eng. C 69 (2016) 154–159.

[4] Y. Chen, D. Kent, M. Bermingham, A. Dehghan-Manshadi, G. Wang, C. Wen, M. Dargusch, Manufacturing of graded titanium scaffolds using a novel space holder technique, Bioactive Mater. 2 (4) (2017) 248–252.

[5] H.D. Jung, T.S. Jang, L. Wang, H.E. Kim, Y.H. Koh, J. Song, Novel strategy for mechanically tunable and bioactive metal implants, Biomaterials 37 (2015) 49–61.

[6] B. Arifvianto, J. Zhou, Fabrication of metallic biomedical scaffolds with the space holder method: a review, Materials 7 (2014) 3588–3622.

[7] C. Gao, C. Wang, H. Jin, Z. Wang, Z. Li, C. Shi, Y. Leng, F. Yang, H. Liu, J. Wang, Additive manufacturing technique-designed metallic porous implants for clinical application in orthopedics, Royal Soc. Chem. 8 (2018) 25210–25227.

[8] M.qi. Cheng, T. Wahafu1, G.f. Jiang, W. Liu, Y.q. Qiao, X.ch. Peng, T. Cheng, X.l. Zhang, G. He, X.y. Liu, A novel open-porous magnesium scaffold with controllable microstructures and properties for bone regeneration, Sci. Rep. 6 (2016) 24134.

[9] S. Toghyani, M. Khodaei, Fabrication and characterization of magnesium scaffold using different processing parameters, Mater. Res. Express 5 (3) (2018) 035407.

[10] S. Toghyani, M. Khodaei, Modified spacer removal and optimum sintering temperature for porous magnesium scaffold fabrication, J. Tissues Mater. 2 (2) (2019) 48–57.

[11] J.M. Rúa, A.A. Zuleta, J. Ramírez, P. Fernández-Morales, Micro-arc oxidation coating on porous magnesium foam and its potential biomedical applications, Surf. Coatings Technol. 360 (2018) 213–221.

[12] M.H. Kang, H.D. Jung, S.W. Kim, S.M. Lee, H.E. Kim, Y. Estrin, Y.H. Koh, Production and bio-corrosion resistance of porous magnesium with hydroxyapatite coating for biomedical applications, Mater. Lett. 108 (2013) 122–124.

[13] S. Dutta, K.B. Devi, M. Roy, Processing and degradation behavior of porous magnesium scaffold for biomedical applications, Adv. Powder Technol. 28 (12) (2017) 3204–3212.

[14] E. Aghion, Y. Perez, Effects of porosity on corrosion resistance of Mg alloy foam produced by powder metallurgy technology, Mater. Charact. 96 (2014) 78–83.

[15] C. Gao, S. Peng, P. Feng, C. Shuai, Bone biomaterials and interactions with stem cells: review, Bone Res. 5 (2017) 17059.

[16] W. Yu, H. Zhao, Z. Ding, Z. Zhang, B. Sun, J. Shen, S. Chen, B. Zhang, K. Yang, M. Liu, D. Chen, Y. He, In vitro and in vivo evaluation of MgF_2 coated AZ31 magnesium alloy porous scaffolds for bone regeneration, Colloids Surf. B: Biointerfaces 149 (2017) 330–340.

[17] M. Yazdimamaghani, M. Razavi, D. Vashaee, L. Tayebi, Development and degradation behavior of magnesium scaffolds coated with polycaprolactone for bone tissue engineering, Mater. Lett. 132 (2014) 106–110.

[18] M. Yazdimamaghani, M. Razavi, D. Vashaee, L. Tayebi, Surface modification of biodegradable porous Mg bone scaffold using polycaprolactone/bioactive glass composite, Mater. Sci. Eng. C 49 (2015) 436–444.

[19] M. Yazdimamaghani, M. Razavi, D. Vashaee, V.R. Pothineni, J. Rajadas, L. Tayebi, Significant degradability enhancement in multilayer coating of polycaprolactone-bioactive glass/gelatin-bioactive glass on magnesium scaffold for tissue engineering applications, Appl. Surf. Sci. 338 (2015) 137–145.

[20] M.H. Kang, H. Lee, T.S. Jang, Y.J. Seong, H.E. Kim, Y.H. Koh, J. Song, H.D. Jung, Biomimetic porous Mg with tunable mechanical properties and biodegradation rates for bone regeneration, Acta Biomater. 84 (2019) 453–467.

[21] T.F.d. Conceicao, N. Scharnag, Fluoride conversion coatings for magnesium and its alloys for the biological environment, Book: Surface Modification of Magnesium and Its Alloys for Biomedical Applications, 2 2015, pp. 3–21 Chapter 1.

[22] K.Y. Chiu, M.H. Wong, F.T. Cheng, H.C. Man, Characterization and corrosion studies of fluoride conversion coating on degradable Mg implants, Surf. Coatings Technol. 202 (2007) 590–598.

[23] H.R. Bakhsheshi-Rad, M. Hasbullah Idris, M.R. Abdul Kadir, M. Daroonparvar, Effect of fluoride treatment on corrosion behavior of Mg-Ca binary alloy for implant application, Trans. Nonferrous Metals Soc. China 23 (2013) 699–710.

[24] E. Gentleman, M.M. Stevens, R.G. Hill, D.S. Brauer, Surface properties and ion release from fluoride-containing bioactive glasses promote osteoblast differentiation and mineralization in vitro, Acta Biomater. 9 (2013) 5771–5779.

[25] E. Moradi, M. Ebrahimian-Hosseinabadi, M. Khodaei, S. Toghyani, Magnesium/nano-hydroxyapatite porous biodegradable composite for biomedical applications, Mater. Res. Express 6 (2019) 075408.

[26] C.E. Wen, M. Mabuchi, Y. Yamada, K. Shimogima, Y. Chino, T. Asahina, Processing of biocompatible porous Ti and Mg, Scripta Mater. 45 (2001) 1147–1153.

[27] G.L. Hao, F.S. Han, W.D. Li, Processing and mechanical properties of magnesium foams, J. Porous. Mater. 16 (2009) 251–256.
[28] A. Hassani, A. Habibolahzadeh, H. Bafti, Production of graded aluminum foams via powder space holder technique, Mater. Des. 40 (2012) 510–515.
[29] L. Stanev, M. Kolev, B. Drenchev, L. Drenchev, Open-cell metallic porous materials obtained through space holders-part I: production methods. A review, J. Manuf. Sci. Eng. 139 (5) (2017) 50801.
[30] A. Vahid, P. Hodgson, Y. Li, New porous Mg composites for bone implants, J. Alloys Compd. 724 (2017) 176–186.
[31] M. Khodaei, M. Meratian, O. Savabi, Effect of spacer type and cold compaction pressure on structural and mechanical properties of porous titanium scaffold, Powder Metall. 58 (2) (2015) 152–160.
[32] I. Mutlu, E. Oktay, Processing and properties of highly porous 17-4 PH stainless steel, Powder Metallurgy Metal Ceramics 50 (1–2) (2011) 73–82.
[33] J.E. House, A TG study of the kinetics of decomposition of ammonium carbonate and ammonium bicarbonate, Thermochim. Acta 40 (1980) 225–233.
[34] H. Langer, H. Offermann, On the solubility of sodium chloride in water, Crystal Growth 60 (1982) 389–392.
[35] Standard A. G1-90, Standard Practice for Preparing, Cleaning and Evaluating Corrosion Test Specimens, ASTM, West Conshohocken PA, USA, 1999.
[36] J.W. Lee, L.C. Thomas, J. Jerrell, H. Feng, K.R. Cadwallader, S.J. Schmidt, Investigation of thermal decomposition as the kinetic process that causes the loss of crystalline structure in sucrose using a chemical analysis approach (part II), J. Agric. Food Chem. 59 (2011) 702–712.
[37] G. Adamek, J. Jakubowicz, Tantalum foam made with sucrose as a space holder, Int. J. Refract. Met. Hard Mater. 53 (2015) 51–55.
[38] J. Zhang, N. Kong, J. Niu, Y. Shi, Haiyan Li, Y. Zhou, G. Yuan, Influence of fluoride treatment on surface properties, biodegradation and cytocompatibility of Mg-Nd-Zn-Zr alloy, J. Mater. Sci. Mater. Med. 25 (2014) 791–799.
[39] P. Makkar, H.J. Kang, A.R. Padalhin, I. Park, B.Gi. Moon, B.T. Lee, Development and properties of duplex MgF_2/PCL coatings on biodegradable magnesium alloy for biomedical applications, PLoS One 13 (4) (2018) 0193927.
[40] T. Yan, L. Tan, D. Xiong, X. Liu, B. Zhang, K. Yang, Fluoride treatment and in vitro corrosion behavior of an AZ31B magnesium alloy, Mater. Sci. Eng. C 30 (2010) 740–748.
[41] K. Chen, Y.Y. Jie, L. Chang, Oxidation characteristics of MgF_2 in air at high temperature, Mater. Sci. Eng. 170 (2017) 012035.
[42] Q.B. Nguyen, M.L.S. Nai, A.S. Nguyen, S. Seetharaman, E.W.W. Leong, M. Gupta, Synthesis and properties of light weight magnesium-cenosphere composite, Mater. Sci. Technol. 32 (9) (2016) 923–929.
[43] R. Karpiński, Ł. Jaworski, P. Czubacka, The structural and machanical properties of the bone, J. Technol. Exploitation Mech. Eng. 3 (1) (2017) 43–50.
[44] M. Taheri Andani, N. Shayesteh Moghaddam, C. Haberland, D. Dean, M.J. Miller, M. Elahinia, Metals for bone implants, part 1: powder metallurgy and implant rendering, Acta Biomater. 10 (10) (2014) 4058–4070.
[45] C.E. Wen, Y. Yamada, K. Shimojima, Y. Chino, H. Hosokawa, M. Mabuchi, Compressibility of porous magnesium foam: dependency on porosity and pore size, Mater. Lett. 58 (2004) 357–360.
[46] X. Zhang, X.W. Li, J.G. Li, X.D. Sun, Preparation and mechanical property of a novel 3D porous magnesium scaffold for bone tissue engineering, Mater. Sci. Eng. C 42 (2014) 362–367.
[47] L. Mao, G. Yuan, J. Niu, Y. Zong, W. Ding, In vitro degradation behavior and biocompatibility of Mg–Nd–Zn–Zr alloy by hydrofluoric acid treatment, Mater. Sci. Eng. C 33 (2013) 242–250.
[48] H. Zhuang, Y. Han, A. Feng, Preparation, mechanical properties and in vitro biodegradation of porous magnesium scaffolds, Mater. Sci. Eng. C 28 (2008) 1462–1466.
[49] A.P.M. Saad, N. Jasmawati, M.N. Harun, M.R. Abdul Kadir, H. Nur, H. Hermawan, A. Syahrom, Dynamic degradation of porous magnesium under a simulated environment of human cancellous bone, Corros. Sci. 112 (2016) 495–506.
[50] M.S. Uddin, C. Hall, P. Murphy, Surface treatments for controlling corrosion rate of biodegradable Mg and Mg-based alloy implants, Sci. Technol. Adv. Mater. 16 (5) (2015) 1–24.
[51] L.E. Monfoulet, P. Becquart, D. Marchat, K. Vandamme, M. Bourguignon, E. Pacard, V. Viateau, H. Petite, D. Logeart-Avramoglou, The pH in the microenvironment of human mesenchymal stem cells is a critical factor for optimal osteogenesis in tissue-engineered constructs, Tissue Eng. A (13–14) (2014) 1827–1840.
[52] Y. Song, S. Zhang, J. Li, C. Zhao, X. Zhang, Electrodeposition of Ca-P coatings on biodegradable Mg alloy: in vitro biomineralization behavior, Acta Biomater. 6 (2010) 1736–1742.
[53] E.C. Meng, S.K. Guan, H.X. Wang, L.G. Wang, S.J. Zhu, J.H. Hu, C.X. Ren, J.H. Gao, Y.S. Feng, Effect of electrodeposition modes on surface characteristics and corrosion properties of fluorine-doped hydroxyapatite coatings on mg-Zn-Ca alloy, Appl. Surf. Sci. 257 (2011) 4811–4816.